Saudi Journal of Biological Sciences 28 (2021) 1196–1202

Contents lists available at ScienceDirect

Saudi Journal of Biological Sciences

journal homepage: www.sciencedirect.com

Original article

Mn_3O_4 nanoparticles: Synthesis, characterization and their antimicrobial and anticancer activity against A549 and MCF-7 cell lines

Mohammed Rafi Shaik [a,*], Rabbani Syed [b,c], Syed Farooq Adil [a], Mufsir Kuniyil [a], Mujeeb Khan [a], Mohammed S. Alqahtani [b,c], Jilani P. Shaik [d], Mohammed Rafiq H. Siddiqui [a], Abdulrahman Al-Warthan [a], Mohammed A.F. Sharaf [e], Abdelatty Abdelgawad [e], Emad Mahrous Awwad [f]

[a] Department of Chemistry, College of Science, King Saud University, P.O. Box 2455, Riyadh 11451, Saudi Arabia
[b] Department of Pharmaceutics, College of Pharmacy, King Saud University, P.O. Box 2457, Riyadh 11451, Saudi Arabia
[c] Nanomedicine & Biotechnology Research Unit, Department of Pharmaceutics, College of Pharmacy, King Saud University, Riyadh 11451, Saudi Arabia
[d] Department of Biochemistry, College of Science, King Saud University, P.O. Box 2455, Riyadh 11451, Saudi Arabia
[e] Department of Industrial Engineering, College of Engineering, King Saud University, P.O. Box 800, Riyadh 11421, Saudi Arabia
[f] Department of Electrical Engineering, College of Engineering, King Saud University, P.O. Box 800, Riyadh, Saudi Arabia

ARTICLE INFO

Article history:
Received 10 November 2020
Revised 26 November 2020
Accepted 30 November 2020
Available online 8 December 2020

Keywords:
Mn_3O_4
Nanoparticles
Antimicrobial
Anticancer activity
A549
MCF-7

ABSTRACT

Due to their inexpensive and eco-friendly nature, and existence of manganese in various oxidation states and their natural abundance have attained significant attention for the formation of Mn_3O_4 nanoparticles (Mn_3O_4 NPs). Herein, we report the preparation of Mn_3O_4 nanoparticles using manganese nitrate as a precursor material by utilization of a precipitation technique. The as-prepared Mn_3O_4 nanoparticles (Mn_3O_4 NPs) were characterized by using X-ray powder diffraction (XRD), UV–Visible spectroscopy (UV–Vis), High-Resolution Transmission electron microscopy (HRTEM), Field emission scanning electron microscopy (FESEM), Thermal gravimetric analysis (TGA) and Fourier-transform infrared spectroscopy (FT-IR). The antimicrobial properties of the as-synthesized Mn_3O_4 nanoparticles were investigated against numerous bacterial and fungal strains including *S. aureus, E. coli, B. subtilis, P. aeruginosa, A. flavus and C. albicans*. The Mn_3O_4 NPs inhibited the growth of *S. aureus* with a minimum inhibitory concentration (MIC) of 40 μg/ml and *C. albicans* with a MIC of 15 μg/ml. Furthermore, the Mn_3O_4 NPs anti-cancer activity was examined using MTT essay against A549 lung and MCF-7 breast cancer cell lines. The Mn_3O_4 NPs revealed significant activity against the examined cancer cell lines A549 and MCF-7. The IC_{50} values of Mn_3O_4 NPs with A549 cell line was found at concentration of 98 μg/mL and MCF-7 cell line was found at concentration of 25 μg/mL.

1. Introduction

Now a day's nanotechnology attained a great interest due to the recent developments in the science and engineering fields, nanotechnology can be deliberated as technology of future (Havancsak, 2003; Hulla et al., 2015; Kumar et al., 2020; Poole Jr and Owens, 2003; Weiss, 2010). Nanotechnology developed numerous types of materials at nanoscale level. In current years, quick advancement in the nanotechnology field has facilitated the development of engineered nanoparticles of different kinds, dimensions, and morphologies (Henry, 2005; Kuhlbusch et al., 2011). Nanoparticles are extensive kinds of materials that embrace particulate materials, which have one dimension below 100 nm at least (Cele, 2020). They can maintain physico-chemical properties such as high surface area, conductance, homogeneity, structural stability or distinct optical properties etc., that make them required in materials science and various application fields (Kung and Kung, 2004; Nabi et al., 2020; Nie et al., 2007).

These nanoparticles have made a tremendous impact in the various applications such as catalysis, pharmaceutics, optics, food technology, cosmetics, water treatment, electrochemistry, energy, biomedicine, biosensor cancer treatment, healthcare and drug delivery (Al-Hobaib et al., 2015; Bae et al., 2006; Dreaden et al.,

* Corresponding author.
E-mail address: mrshaik@ksu.edu.sa (M.R. Shaik).
Peer review under responsibility of King Saud University.

Production and hosting by Elsevier

https://doi.org/10.1016/j.sjbs.2020.11.087
1319-562X/

2012; El-Sayed and Kamel, 2020; Kung and Kung, 2003; Mu and Sprando, 2010; Ndlovu et al., 2020). The nanoparticles properties in the medicinal arena were improved greater associated to their bulk counterparts. In this nanomaterial's metal and metal oxide nanoparticles display distinct physical and chemical properties, particularly metal oxide nanomaterial's are enormously stimulating in the field of semiconducting constituents and endorse an ideal prospect for the progress of biological activities (Charbgoo et al., 2017; Mirzaei and Darroudi, 2017). In these nanomaterials, trimangnese tetraoxide nanoparticles (Mn_3O_4) is one of the significant nanoparticles comprise of various crystal structures constructed from octahedral MnO_6 were, manganese dioxide (MnO_2), dimanganese trioxide (Mn_2O_3) and trimangnese tetraoxide nanoparticles (Mn_3O_4) (Deka et al., 2020; Jiang et al., 2020; Roche et al., 2007; Shin et al., 2009; Yang et al., 2010).

There are a diversity of approaches to develop metal/metal oxide NPs, for instance precipitation, hydrothermal, microemulsion, sol–gel, and sonochemical technique, which usually provide adequate products for various applications (Ghazal et al., 2020; Medhi et al., 2020; Yadav et al., 2020). Manganese oxides is a mixed oxide material are appropriate for wide range applications such as catalysis, electrochemical, medicinal due to their low cost, eco-friendly nature, existence of manganese in various states and their natural abundance (Hoseinpour and Ghaemi, 2018; Kumar et al., 2017; Wang et al., 2017). The numerous manganese oxidation states consequences in the development of manganese dioxide, dimanganese trioxide, trimanganese tetraoxide. In these, Mn_3O_4 nanoparticles have encouraged abundant attention owing to their distinctive structural and electronic features with exclusive ion exchange, catalysis, molecular adsorption, magnetic and electrochemical properties. Manganese is deliberated a vital constituent in metabolism has been well controlled by biological systems and Mn_3O_4 NPs display greater biological properties and low toxicity (Bhattacharya et al., 2019; Khan et al., 2016). Accordingly, Mn_3O_4 NPs have been competently examined as prospective antibacterial systems because of their synergistic performance. The ions 'Mn^{2+}' generates harmless free radicals, which performance a vital part in clinical sicknesses like Alzheimer's, cardiac, diabetes, numerous diseases etc., including cancer, and moreover, nanomedicine is supposed to be a favorable investigation route in the tumors treatment (Khan et al., 2016).

In the current scenario, the major complication in cancer treatment is the partial existence of particular anticancer drugs or nanomedicines along with a lesser amount of competent delivery systems and majority of the currently existing anticancer drugs having poor solubility in aqueous solutions. Consequently, major efforts have been carried out to generate novel anticancer drugs with superior aqueous solubility and effective in cancer treatment. Among them, metal oxide nanoparticles have synergistic and superior physicochemical properties made huge attention in cancer treatment (Behzadi et al., 2019; Khan et al., 2016; Pugazhendhi et al., 2019).

In the current work, we demonstrate a precipitation method for the synthesis Mn_3O_4 nanoparticles using manganese nitrate as a precursor material by utilization of a precipitation method (Scheme 1). As-synthesized Mn_3O_4 nanoparticles characterized by several microscopic, spectroscopic and thermal techniques such as HRTEM, FESEM, EDX, UV–Vis, XRD, FT-IR, and TGA. The biological properties of the as-prepared Mn_3O_4 NPs were investigated against various fungal and bacterial strains comprising *S. aureus, B. subtilis, E. coli*, *P. aeruginosa, C. albicans and A. flavus*. The growth of *S. aureus* inhibited with a MIC of 40 μg/ml and *C. albicans* with a MIC of 15 μg/ml using Mn_3O_4 NPs. Furthermore, the Mn_3O_4 NPs anti-cancer activity was examined using MTT essay against A549 lung and MCF-7 breast cell lines. The Mn_3O_4 NPs revealed significant activity against the investigated cancer cell lines A549 and MCF-7.

2. Materials and methods

2.1. Materials

All chemicals, such as Manganese nitrate, sodium bicarbonate, phosphate buffer saline, dimethyl sulfoxide, and all other materials and organic solvents were procured from Sigma Aldrich (USA).

2.2. Synthesis of Mn_3O_4 nanoparticles

Mn_3O_4 was prepared by precipitation method. 0.1 M Manganese nitrate (100 mL) was prepared in distilled water and transferred to a reaction vessel and the heating of the reaction vessel was increased to 90 °C under mechanical stirring. Once the temperature is attained 0.05 M sodium bicarbonate is added dropwise to attain the pH 9. At pH 9 stopped the addition of sodium bicarbonate and heated another 3 h under continuous stirring. After 3 h, the reaction vessel brought down to room temperature and stirred further overnight. The reaction mixture was washed using centrifugation and dried at 70 °C overnight. The attained powder was calcined at 600 °C for12 hours to achieve Mn_3O_4 nanoparticles.

2.3. Characterization

The as-prepared Mn_3O_4 NPs are characterized by several approaches. The XRD characterization is carried out using Bruker diffractometer (Cu Kα, (λ = 1.5406 Å)). The spectral characterization was carried out using PerkinElmer UV–Vis spectrometer and Bruker IFS 66 v/S spectrometer are used for UV–Vis and FT-IR spectral analysis, respectively. The microscopic analysis such as FESEM is carried to understand the surface analysis is analysed out by FESEM (JED-2200, JEOL, Tokyo, Japan) and the FESEM sample was fixed onto a stub with carbon-built dual-sided adhesive tape and then sputter coated with nearly 10 nm of platinum. For imaging, the sample is focused on perpendicular to the inward electron beam. FESEM pictures were captured using an operational voltage of 5 kV and a working distance of 4.5 mm over several magnifications. HRTEM was performed on a JEOL JEM 2100 PLUS, (USA). The sample for HRTEM analysis was prepared by placing a drop of primary sample on a holy carbon copper grid, which were dried in oven for 6 h at 80C°. HRTEM images are recorded with operating at 200 kV accelerating voltage. Thermo gravimetric analysis was analyzed using Metler Toledo instrument, TGA/DSC1, Im Langacher, Switzerland.

2.4. Antibacterial and antifungal activity of the of the as-synthesized Mn_3O_4 nanoparticles

The antimicrobial activity of NPs was accomplished using the conventional agar disk diffusion and MIC approaches. Six American Type Culture Collection bacterial and fungal strains, namely *E. coli*, *S. aureus*, *B. subtilis, P. aeruginosa* and two fungal strains *C. albicans and A. flavus* were acquired from the Microbiology Department, Pharmacy College, King Saud University. All the bacterial and fungal strains were sub-cultured in newly made nutrient broth and post observation of growth was consistent as per 0.5 McFarland turbidity standards. The inoculum was plated on nutrient agar plates by the spread plate procedure and a sterile borer six mm was cast-off to bore four wells in the ready plate. Each wells, 100 μL of 30 μg/mL each of Mn_3O_4 NPs, gentamycin & fluconazole (50 μg/mL) was added and the fourth well persisted as the '-ve'

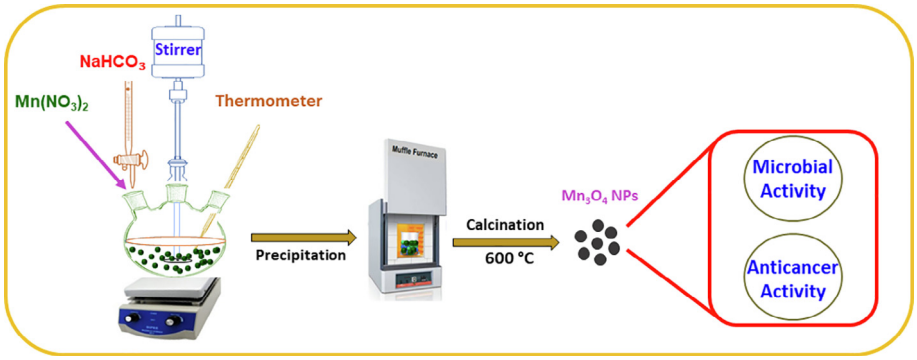

Scheme 1. Graphical representation of as-prepared Mn_3O_4 NPs using sodium bicarbonate and assessment of their antimicrobial and anticancer activity.

control. The cultured plates were incubated at 37 ℃ for 24 h to check the inhibition zone of tested bacteria 24 h for bacterial strains and for 48 h for tested fungal strains. All the test were done in triplicates to rule out false positive results

2.5. Epsilometer test for MIC analysis

To determine MIC, Standard McFarland inoculum was prepared using Muller Hilton broth using overnight grown culture of the tested strains. 100 μg/ml Mn_3O_4 NPs was added to the broth solution containing the standard culture and incubated at optimum temperature and time as for the previous protocol (Hannan et al., 2020). The Muller Hilton agar plates were swabbed with the broth inoculum containing the Mn_3O_4 NPs. The plates were seeded with E strip containing gradient concentration of standard antibiotic of gentamycin for antibacterial and fluconazole for anti-fungal analysis. After incubation MIC was recorded. All the tests were done in triplicates to rule out false positive results

2.6. Cytotoxic activity Mn_3O_4 NPs

The as-prepared Mn_3O_4 NPs was employed to investigate the anticancer activity of human lung and breast A549 and MCF-7 cell lines. Both cell lines cultured in Dulbecco's Modified Eagle Medium with fetal bovine serum (7%) and each penicillin & streptomycin (1%). The cell culturing was prepared at 37 °C in 5% CO_2 supply incubator. The sub culturing was completed at regular intermission for every round of analysis. The exponential growing cells were exploited.

MTT colorimetric assay (3-[4,5-dimethylthiazole-2-y]-2,5-diph enyltetrazolium bromide) method was used to examine the both cancer cell lines. The IC_{50} values of both A549 and MCF-7 were assessed by the cytotoxicity assessment using Mn_3O_4 NPs. All cell suspension of about 5×10^4 cells were sowed in a 96-well flat plate comprising Dulbecco's Modified Eagle Medium with fetal bovine serum (5%) and various concentrations of Mn_3O_4 NPs: 0, 25, 50, 75 and 100 μg/mL. The mixture was kept in 5% CO_2 incubator for a time of 24 h. After incubation period, the subjected cells to a wash serum free medium and a 100 mL of 5 μg/mL of MTT solution was added pursued by incubation period for 4 to 5 h. After post incubation, the both cell lines were again processed and cleaned with buffer phosphate, and dimethyl sulfoxide 100 μL was added to solubilize the unbound formazan. The plates were assessed at an absorbance of 570 nm in a plate reader. The whole tests were performed in triplicates. The IC_{50} was estimated by the intensity of the color produced formazan dye comparably to the number of viable cells in the well. The IC_{50} value was defined as the concentration of tested compound needed to inhibit 50% of cells growth.

3. Results

3.1. UV–Visible analysis

Primarily, the Mn_3O_4 nanoparticle development was examined via UV–Visible analysis, Fig. 1. exhibits the UV–Vis spectra of as-prepared Mn_3O_4 nanoparticle using manganese nitrate. The UV–Vis spectra of Mn_3O_4 nanoparticles characteristic peak at ~ 220 nm clearly indicating the Mn_3O_4 nanoparticle formation.

3.2. XRD analysis

The crystallinity of Mn_3O_4 NPs attained via precipitation method was identified using XRD analysis as presented in Fig. 2. The as-synthesized Mn_3O_4 NPs exhibited tetragonal structure (hausmannite, *I*41/*amd*) with constant lattice values '*a*' = 0.5746 nm and '*c*' = 0.9463 nm. These values are reliable with the previous report attained by other investigator values for Mn_3O_4 NPs (JCPDS No.24–0734), which is clearly replicated by the existence of fourteen characteristic peaks in the XRD pattern such as, 18.2° (101), 29.1° (112), 31.2° (200), 32.5° (103), 36.3° (211), 38.2° (004), 44.6° (220), 50.8° (105), 53.8° (312), 55.3° (303), 58.7° (321), 60.0° (224), 64.8° (314), 74.3° (413). No further additional impurities peaks noticed in XRD analysis i.e. clearly indicating the no other forms of manganese oxides were noticed. Furthermore, the Debye–Scherrer formula was used to estimate average crystallite size (Table 1).

"d" space calculated for tetragonal structure

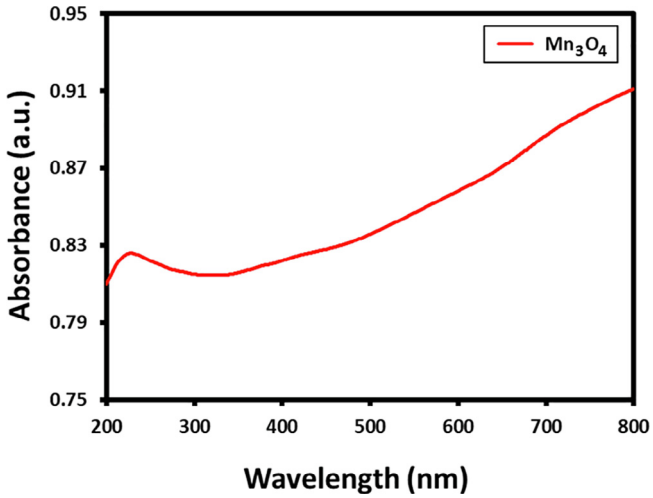

Fig. 1. UV–Vis absorption spectra of Mn_3O_4 nanoparticles.

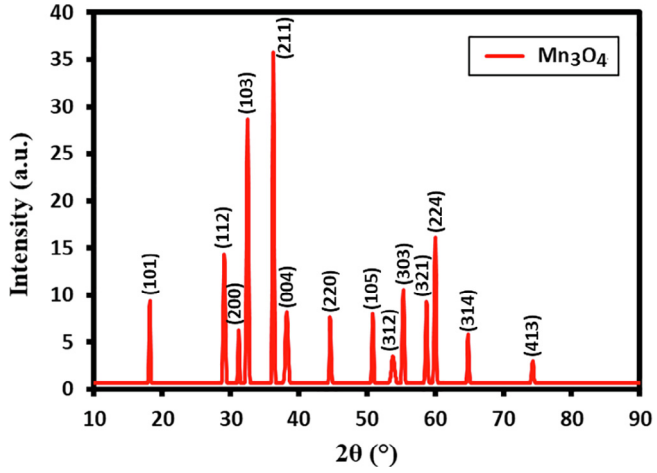

Fig. 2. XRD diffractograms of Mn_3O_4 nanoparticles.

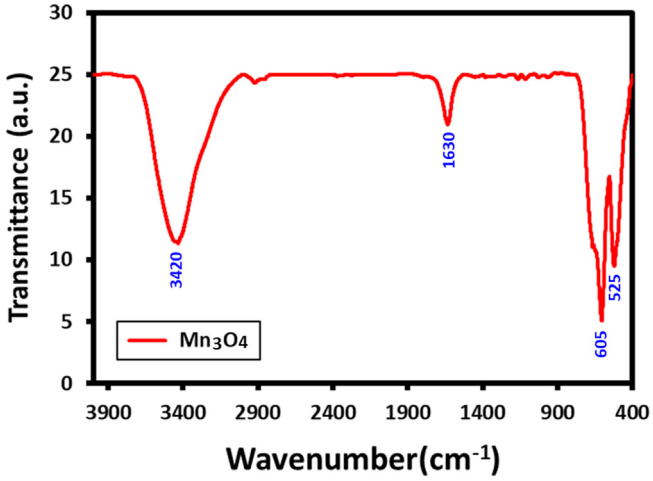

Fig. 3. FT-IR spectrum of the as-synthesized Mn_3O_4 nanoparticles.

$$\frac{1}{d^2} = \frac{h^2 + k^2}{a^2} + \frac{l^2}{c^2}$$

Where, *a, c* = Lattice Constants, 'd' is Interplanar Spacing, h, k, l = Miller Indices;

Debye–Scherrer formula, $\mathbf{D} = \frac{k\lambda}{\beta\cos\theta}$

'D' is the Crystal size, 'λ'- is corresponding to wavelength X-ray, and 'k'dimensionless shape factor, 'β' is the line broadening at half the maximum intensity, 'θ' is Bragg's angle.

The average crystallite size is found to be 36 nm, which is little higher when compare to the size of the particles obtained by TEM. This is due the slight deviation from the ideal shape of the particles considered in the Debye–Scherer formula.

3.3. FT-IR analysis

Fig. 3. displays the FTIR spectra of as-synthesized Mn_3O_4 NPs, the 'Mn' and 'O' bonding state in the Mn_3O_4 NPs was investigated with the FTIR analysis. The Mn_3O_4 FTIR spectra displayed several characteristic peaks at lower region bands of Mn-O comprising the peaks between 400 and 650 cm^{-1}. However, the characteristic peak of Mn-O, stretching modes occurred in the range of 624 cm^{-1}. The significant peak positioned at 624 cm^{-1} was characteristic of Mn-O stretching modes in tetragonal sites. While the vibrational frequency poisoned at 525 cm^{-1} associated to the Mn-O distortion vibration. Furthermore, the characteristic narrow band and broad band situated at 3420 and 1600 cm^{-1} were corresponded to the hydroxy (OH) should be absorbed by the samples or KBr. These FT-IR analysis outcomes are reliable with the evidence achieved from further performed characterization outcomes.

3.4. TGA analysis

Thermal stability of the Mn_3O_4 nanoparticles were performed under 'N_2' atmosphere at a heating rate of 10℃/min. TGA of the as-synthesized Mn_3O_4 NPs sample shows thermal stability of the Mn_3O_4 NPs presented in this Fig. 4. The Mn_3O_4 NPs shows no significant weight loss in this temperature range to 800 ℃, as all organic residues have been removed, that discloses the stability of attained Mn_3O_4 nanoparticles.

3.5. HRTEM and EDX analysis

The as-synthesized Mn_3O_4 NPs size and shape was investigated by HRTEM analysis (Fig. 5(a)). The HRTEM results displays the uniformly distributed nanoparticles within a size approximately 35–40 nm. Though, the bulk of the NPs in the HRTEM images are less than 35 nm in size. Moreover, the composition of elements in the as-synthesized Mn_3O_4 NPs was also determined by energy dispersive X-ray spectroscopy analysis (EDX). The EDX analysis revealed that 'Mn' and 'O' is the main elements in the attained product, which was determined by the occurrence of strong intense peaks at 0.6, 5.8, and 6.4 keV corresponding to 'Mn' and 0.5 keV intense signal belongs to 'O', which is due to an optical absorption in this region due to the surface Plasmon resonance (SPR). Consequently, The EDX analysis authorized the development of Mn_3O_4 NPs (Fig. 5

Table 1
XRD results and crystallographic data of the Mn_3O_4 nanoparticles.

2θ (°)	d space (nm)	h,k,l	a (nm)	c (nm)	Crystal size (D) (nm)
18.2	0.49	101	0.5746	0.9463	45.45258
29.1	0.31	112	0.5746	0.9463	31.16673
31.2	0.29	200	0.5746	0.9463	47.01039
32.5	0.28	103	0.5746	0.9463	31.99853
36.3	0.25	211	0.5746	0.9463	40.4086
38.2	0.24	004	0.5746	0.9463	23.22652
44.6	0.20	220	0.5746	0.9463	38.23237
50.8	0.18	105	0.5746	0.9463	42.44687
53.8	0.17	312	0.5746	0.9463	20.28826
55.3	0.16	303	0.5746	0.9463	33.65284
58.7	0.16	321	0.5746	0.9463	35.47193
60.0	0.15	224	0.5746	0.9463	37.4525
64.8	0.14	314	0.5746	0.9463	42.27171
74.3	0.13	413	0.5746	0.9463	37.38172

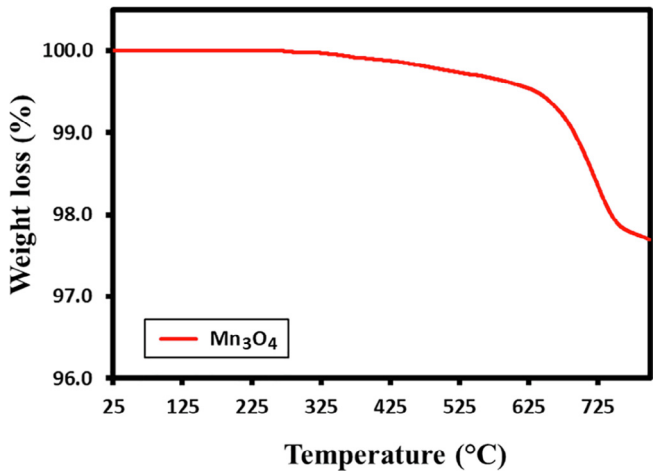

Fig. 4. TGA analysis of Mn_3O_4 nanoparticles.

(b)). The particle size distribution graph was attained from TEM image using Image J software. Crystallite size attained from the XRD analysis is approximately similar to the particle size attained from the TEM analysis (Fig. 5(c)).

3.6. FESEM and EDX results

The surface structure and size of the as-prepared Mn_3O_4 NPs were further scrutinized using Field emission Scanning Electron Microscopy (FESEM). Fig. 6, designates that the original surface morphology of the Mn_3O_4 NPs is flakes with the diameter about below 100 nm. Aggregated Mn_3O_4 NPs is in the form of flakes. Based on the previously reported literature it can be assumed that the flakes like morphology corresponding to the Mn_3O_4 NPs are observed, and their diameter varies between 30 and 40 nm. The FESEM results of the Mn_3O_4 nanoparticles agree with the XRD data. The EDX analysis revealed that 'Mn' and 'O' is the main elements in the attained product, which was determined by the occurrence of strong intense peaks at 0.6, 5.8, and 6.4 keV corresponding to 'Mn' and 0.5 keV intense signal belongs to 'O', which is due to an optical absorption in this range due to the SPR. Consequently, The EDX analysis revealed that 'Mn' and 'O' is the main elements in the attained product, which was determined by the occurrence of strong intense peaks at 0.6, 5.8, and 6.5 keV corresponding to 'Mn' and 0.5 keV intense signal belongs to 'O'. The attained EDX analysis confirmed the formation of Mn_3O_4 NPs.

3.7. Antimicrobial activity of the Mn_3O_4 NPs

The Mn_3O_4 nanoparticle's microbial properties of were examined using the disk diffusion method including Gram '+ve' and '– ve' organisms such as *E. coli*, *B. subtilis*, *S. aureus*, and *P. aeruginosa.* The activity of Mn_3O_4 was matched with the Gentamycin. For the Gram + ve organisms, Mn_3O_4 nanoparticles showed a similar zone of inhibition resultant to well-known antibiotic Gentamycin. Mn_3O_4 NPs shown resistance towards bacterial strains both for *E. coli* and *P. aeruginosa* with zone of inhibition 10 mm & 12 mm. Gram + ve bacteria *S. aureus* & *B. subtilis* shown susceptibility towards Mn_3O_4 NPs with zone of inhibition 19 mm & 18 mm respectively. The results from the fungal activity showed mixed results where *C. albicans* was susceptible with zone of inhibition 18 mm and *A. flavus* showing intermediate results with zone of inhibition of 13 mm (Table 2).

Further MIC analysis was determined for the susceptible strains using E-test. This is one the advance and cheapest method to evaluate the inhibitory concentration of the drugs. The MIC of nano with *S. aureus* was recorded as 40 μg/ml and with *C. albicans* was recorded to be 15 μg/ml.

3.8. Cytotoxicity results

The Cytotoxicity assessment in terms of IC_{50} was calculated. As shown in Fig. 7. The IC_{50} of Mn_3O_4 NPs with A549 cell lines was found at concentration of 98 μg/mL and IC_{50} of Mn_3O_4 NPs with MCF-7 cell lines was found at concentration of 25 μg/mL. More than 80% growth inhibition was observed in concentrations more than 200 μg/mL. Lower concretions of Mn_3O_4 NPs were working efficient which would be used and compactable in drug delivery systems. Our results clearly indicate that lower concentration of Mn_3O_4 NPs showing efficient activity towards tested two cell lines.

4. Discussion

Development of antimicrobial agents using metallic nanoparticles been proved to be alternative to conventional antibiotics and the results were promising which is of clinical importance (Singh et al., 2020). The antimicrobial activity of Mn_3O_4 NPs and the ability of this nano material inhibiting the microbial growth would be considered for drug formulations in treating various infectious diseases. Kim et al., described that nanoparticles display antimicrobial activity in correlation of the size and concentration of NPs (Kim et al., 2007), perhaps lower activity may also due to lower concentration of NPs. The scenario may somehow consider and has to be correlated with other factors like type of microorganism and optimum conditions. The current study on detecting the antimicrobial

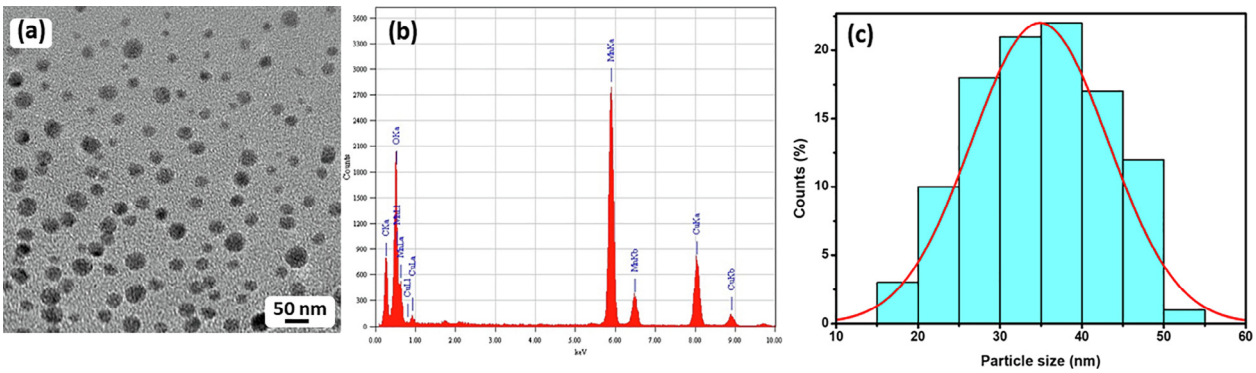

Fig. 5. (a) TEM image of the as-synthesized Mn_3O_4 nanoparticles, (b) energy dispersive X-ray spectroscopy (EDX) of Mn_3O_4 nanoparticles and (c) particle size distribution graph of Mn_3O_4 nanoparticles.

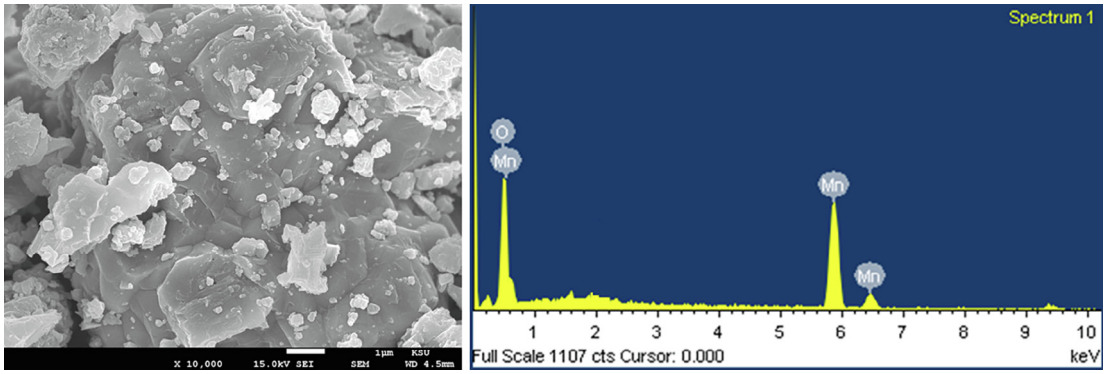

Fig. 6. (a) FESEM image of the as-synthesized Mn_3O_4 nanoparticles and (b) energy dispersive X-ray spectroscopy of Mn_3O_4 nanoparticles.

Table 2
Zone of Inhibition results of the susceptibility of different microbial strains tested against standard antibiotics.

Zone of Inhibition (mm)	Mn_3O_4 NPs	Antibiotic-Gentamycin (30 μg/ml)	Antibiotic-fluconazole (50 μg/ml)
E. coli	10 mm	22 mm	–
S. aureus	19 mm	21 mm	–
P. aeruginosa	12 mm	22 mm	–
B. subtilis	18 mm	22 mm	–
C. albicans	18 mm	–	20 mm
A. flavus	14 mm	–	20 mm

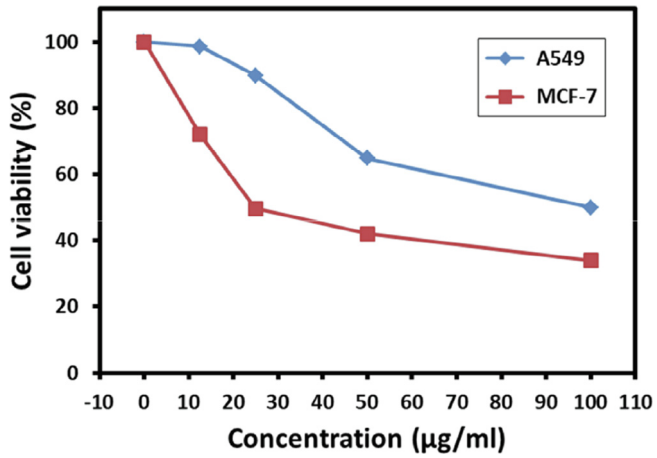

Fig. 7. Viability outcome by MTT assay for Mn_3O_4 NPs.

and anticancer activity of Mn_3O_4 NPs prepared using precipitation approach. Moreover, the as-prepared Mn_3O_4 NPs was characterized using various microscopic, spectroscopic and thermal techniques, comprising UV–Vis, FT-IR XRD, HRTEM, FESEM and TGA. The as-synthesized Mn_3O_4 NPs exhibited tetragonal structure and the average crystallite size is found to be 36 nm, which is little higher when compare to the size of the particles obtained by HRTEM. This is due the slight deviation from the ideal shape of the particles considered in the Debye–Scherer formula. The thermal stability of the Mn_3O_4 NPs displayed no significant weight loss up to 800 °C that discloses the stability of attained Mn_3O_4 nanoparticles. The as-prepared Mn_3O_4 NPs were then scrutinized for antimicrobial activity using disk diffusion process and MIC, however the anticancer activity was examined using human and breast cancer cell lines.

Our antimicrobial results were in agreement with Azhir et al., 2015 where *E. coli* shown to be sensitive and *S. aurues* showing susceptibility towards Mn_3O_4 NPs, whereas reports from (Chowdhury et al., 2009) shown *E. coli* is susceptible. Packirisamy et al., displayed the same results where *B. subtilis* is susceptible and *E. coli* and *P. aeruginosa* also susceptible as anti-microbial activity increased by increasing the concentration (Packirisamy et al., 2019). The Mn_3O_4 NPs inhibited the growth of *S. aureus* with a minimum inhibitory concentration (MIC) of 40 μg/ml and *C. albicans* with a MIC of 15 μg/ml. The results indicate that the as-prepared Mn_3O_4 NPs prepared from manganese nitrate using precipitation approach is a favorable contender for usage pharmaceutical industries and food packaging applications.

The application of nanotechnology in modern medicine has extended the permeability in various approaches in better treatment procedures most importantly in cancer treatment (Ivanković et al., 2003). Many of the previous studies has used different methods in producing Mn_3O_4 NPs to enhance the permeability and also minimize the toxicity as 'Mn' is known for the best catalytic activity (Juzenas et al., 2008). Mn_3O_4 NPs known for its anti-inflammatory (Fu et al., 2020), hepato-protecive (Adhikari et al., 2016) and anti-cancer (Gotić et al., 2009) properties. Our results clearly indicate that lower concentration of Mn_3O_4 NPs showing efficient activity towards tested two cell lines. In our study Mn_3O_4 NPs were made and their anticancer activity was evaluated using human lung cell line (A549) and breast cancer cell line (MCF-7). The IC_{50} investigation accomplished using Mn_3O_4 NPs. Mn_3O_4 NPs showed them A549 cell lines were found at concentration of 98 μg/mL and IC_{50} of Mn_3O_4 NPs with MCF-7 cell lines was found at concentration of 25 μg/mL. The as-prepared Mn_3O_4 NPs were found to be effective against the examined cell and demonstrating their potential use against human lung and breast cancer cell lines.

5. Conclusions

Mn_3O_4 NPs successfully achieved by using precipitation approach. The as-synthesized Mn_3O_4 nanoparticles are uniformly distributed and well dispersed and tetragonal in shape. The characterization of Mn_3O_4 nanoparticles was performed by UV–Vis, FT-IR, TGA, XRD, FESEM, HRTEM and EDX analysis. The results have exposed the development of tetragonal shape with an average size of 36 nm. The prepared Mn_3O_4 nanoparticles were assessed for their biological and anticancer activities. Furthermore, the antibacterial properties, the zone of inhibition, and the minimum inhibitory concentration of Mn_3O_4 nanoparticles displayed the inhibitory effect against all tested bacteria. Though, the Mn_3O_4 nanoparticles were found to be selective against *S. aureus*, & *B. subtilis* gram positive bacterial strains. Both Gram positive bacteria *S. aureus* & *B. subtilis* shown susceptibility towards Mn_3O_4 nanoparticles with zone of inhibition 19 mm and 18 mm respectively. The

results from the antifungal activity exposed mixed results where *C. albicans* was susceptible with zone of inhibition 18 mm and *A. flavus* showing intermediate results with zone of inhibition of 13 mm. additionally, Additionally, the anti-cancer activity of Mn_3O_4 NPs was also studied against A549 lung and MCF-7 breast cancer cell lines by applying MTT assay. The cytotoxicity assessment in terms of IC_{50} was calculated. As revealed the IC_{50} of Mn_3O_4 nanoparticles with A549 was found at concentration of 98 μg/mL and IC_{50} of Mn_3O_4 nanoparticles with MCF −7 cell lines was found at concentration of 25 μg/mL.

Declaration of Competing Interest

The authors declare that they have no known competing financial interests or personal relationships that could have appeared to influence the work reported in this paper.

Acknowledgments

The authors extend their appreciation to the Deanship of Scientific Research at King Saud University for funding this work through research group no. RG-1441-453.

References

Adhikari, A., Polley, N., Darbar, S., Bagchi, D., Pal, S.K., 2016. Citrate functionalized Mn_3O_4 in nanotherapy of hepatic fibrosis by oral administration. Future Sci. OA 2, FSO146.
Al-Hobaib, A.S., Al-sheetan, K.M., Shaik, M.R., Al-Andis, N.M., Al-Suhybani, M., 2015. Characterization and evaluation of reverse osmosis membranes modified with Ag_2O nanoparticles to improve performance. Nanoscale Res. Lett. 10, 379.
Bae, Y., Lee, D.C., Rhogojina, E.V., Jurbergs, D.C., Korgel, B.A., Bard, A.J., 2006. Electrochemistry and electrogenerated chemiluminescence of films of silicon nanoparticles in aqueous solution. Nanotechnology 17, 3791.
Behzadi, E., Sarsharzadeh, R., Nouri, M., Attar, F., Akhtari, K., Shahpasand, K., Falahati, M., 2019. Albumin binding and anticancer effect of magnesium oxide nanoparticles. Int. J. Nanomed. 14, 257.
Bhattacharya, P., Swain, S., Giri, L., Neogi, S., 2019. Fabrication of magnesium oxide nanoparticles by solvent alteration and their bactericidal applications. J. Mater. Chem.: *B* 7, 4141–4152.
Cele, T., 2020. Preparation of Nanoparticles, in: Silver Nanoparticles-Health and Safety. IntechOpen.
Charbgoo, F., Ahmad, M.B., Darroudi, M., 2017. Cerium oxide nanoparticles: green synthesis and biological applications. Int. J. Nanomed. 12, 1401.
Chowdhury, A.-N., Azam, M.S., Aktaruzzaman, M., Rahim, A., 2009. Oxidative and antibacterial activity of Mn_3O_4. J. Hazard. Mater. 172, 1229–1235.
Deka, K., Guleria, A., Kumar, D., Biswas, J., Lodha, S., Kaushik, S.D., Dasgupta, S., Deb, P., 2020. Exclusive T2 MRI contrast enhancement by mesoporous carbon framework encapsulated manganese oxide nanoparticles. Curr. Appl. Phys. 20, 89–95.
Dreaden, E.C., Alkilany, A.M., Huang, X., Murphy, C.J., El-Sayed, M.A., 2012. The golden age: gold nanoparticles for biomedicine. Chem. Soc. Rev. 41, 2740–2779.
El-Sayed, A., Kamel, M., 2020. Advanced applications of nanotechnology in veterinary medicine. Environ. Sci. Pollut. Res. 27, 19073–19086.
Fu, S., He, Z., Tang, Y., Lan, B., 2020. Effect of Mn_3O_4 Nanoparticles on Lipopolysaccharide-Induced Inflammatory Factors in the Human Tendon Cells and Its Mechanism. Int. J. Polym. Sci.
Ghazal, S., Akbari, A., Hosseini, H.A., Sabouri, Z., Forouzanfar, F., Khatami, M., Darroudi, M., 2020. Sol-gel biosynthesis of nickel oxide nanoparticles using Cydonia oblonga extract and evaluation of their cytotoxicity and photocatalytic activities. J. Mol. Struct., 128378
Gotić, M., Ivanković, S., Musić, S., Prebeg, T., 2009. Synthesis of Mn_3O_4 nanoparticles and their application to cancer cells. Collect. Czech. Chem. Commun. 74, 1351–1360.
Hannan, M., Haque, M., Mohibbullah, M., Dash, R., Hong, Y.K., Moon, I.S., 2020. Gelidium amansii Attenuates Hypoxia/Reoxygenation-Induced Oxidative Injury in Primary Hippocampal Neurons through Suppressing GluN2B Expression. Antioxidants 9, 223.
Havancsak, K., 2003. In Nanotechnology at present and its promise for the future. Trans Tech Publ Mater. Sci. Forum, 85–94.
Henry, C.R., 2005. Morphology of supported nanoparticles. Prog. Surf. Sci. 80, 92–116.
Hoseinpour, V., Ghaemi, N., 2018. Green synthesis of manganese nanoparticles: Applications and future perspective–A review. J. Photochem. Photobiol B 189, 234–243.
Hulla, J., Sahu, S., Hayes, A., 2015. Nanotechnology: History and future. Hum. Exp. Toxicol. 34, 1318–1321.
Ivanković, S., Gotić, M., Jurin, M., Musić, S., 2003. Photokilling squamous carcinoma cells SCCVII with ultrafine particles of selected metal oxides. J. Sol-Gel Sci. Technol. 27, 225–233.
Jiang, X., Gray, P., Patel, M., Zheng, J., Yin, J.-J., 2020. Crossover between anti-and pro-oxidant activities of different manganese oxide nanoparticles and their biological implications. J. Mater. Chem.: *B* 8, 1191–1201.
Juzenas, P., Chen, W., Sun, Y.-P., Coelho, M.A.N., Generalov, R., Generalova, N., Christensen, I.L., 2008. Quantum dots and nanoparticles for photodynamic and radiation therapies of cancer. Adv. Drug Deliv. Rev. 60, 1600–1614.
Khan, S., Ansari, A.A., Khan, A.A., Abdulla, M., Al-Obeed, O., Ahmad, R., 2016. In vitro evaluation of anticancer and biological activities of synthesized manganese oxide nanoparticles. MedChemComm 7, 1647–1653.
Kim, J.S., Kuk, E., Yu, K.N., Kim, J.-H., Park, S.J., Lee, H.J., Kim, S.H., Park, Y.K., Park, Y. H., Hwang, C.-Y., 2007. Antimicrobial effects of silver nanoparticles. Nanomed. Nanotechnol. 3, 95–101.
Kuhlbusch, T.A., Asbach, C., Fissan, H., Göhler, D., Stintz, M., 2011. Nanoparticle exposure at nanotechnology workplaces: a review. Part. Fibre Toxicol. 8, 1–18.
Kumar, S., Nehra, M., Kedia, D., Dilbaghi, N., Tankeshwar, K., Kim, K.-H., 2020. Nanotechnology-based biomaterials for orthopaedic applications: Recent advances and future prospects. Mater. Sci. Eng. C 106, 110154.
Kumar, V., Singh, K., Panwar, S., Mehta, S.K., 2017. Green synthesis of manganese oxide nanoparticles for the electrochemical sensing of p-nitrophenol. Int. Nano Lett. 7, 123–131.
Kung, H.H., Kung, M.C., 2003. Heterogeneous catalysis: what lies ahead in nanotechnology. Appl. Catal. A 246, 193–196.
Kung, H.H., Kung, M.C., 2004. Nanotechnology: applications and potentials for heterogeneous catalysis. Catal. Today 97, 219–224.
Medhi, R., Marquez, M.D., Lee, T.R., 2020. Visible-Light-Active Doped Metal Oxide Nanoparticles: Review of their Synthesis, Properties, and Applications. ACS Appl. Nano Mater. 3, 6156–6185.
Mirzaei, H., Darroudi, M., 2017. Zinc oxide nanoparticles: Biological synthesis and biomedical applications. Ceram. Int. 43, 907–914.
Mu, L., Sprando, R.L., 2010. Application of nanotechnology in cosmetics. Pharm. Res. 27, 1746–1749.
Nabi, G., Raza, W., Tahir, M., 2020. Green Synthesis of TiO_2 Nanoparticle Using Cinnamon Powder Extract and the Study of Optical Properties. J. Inorg. Organomet. Polym. Mater. 30, 1425–1429.
Ndlovu, N., Mayaya, T., Muitire, C., Munyengwa, N., 2020. Nanotechnology Applications in Crop Production and Food Systems. Int. J. Plant Breed. 7, 624–634.
Nie, S., Xing, Y., Kim, G.J., Simons, J.W., 2007. Nanotechnology applications in cancer. Annu. Rev. Biomed. Eng. 9, 257–288.
Packirisamy, R.G., Govindasamy, C., Sanmugam, A., Karuppasamy, K., Kim, H.-S., Vikraman, D., 2019. Synthesis and Antibacterial Properties of Novel $ZnMn_2O_4$–Chitosan Nanocomposites. Nanomaterials 9, 1589.
Poole Jr, C.P., Owens, F.J., 2003. Introduction to nanotechnology. John Wiley & Sons.
Pugazhendhi, A., Prabhu, R., Muruganantham, K., Shanmuganathan, R., Natarajan, S., 2019. Anticancer, antimicrobial and photocatalytic activities of green synthesized magnesium oxide nanoparticles (MgONPs) using aqueous extract of Sargassum wightii. J. Photochem. Photobiol. B 190, 86–97.
Roche, I., Chaînet, E., Chatenet, M., Vondrák, J., 2007. Carbon-supported manganese oxide nanoparticles as electrocatalysts for the oxygen reduction reaction (ORR) in alkaline medium: physical characterizations and ORR mechanism. J. Phys. Chem. C 111, 1434–1443.
Shin, J., Anisur, R.M., Ko, M.K., Im, G.H., Lee, J.H., Lee, I.S., 2009. Hollow manganese oxide nanoparticles as multifunctional agents for magnetic resonance imaging and drug delivery. Angew. Chem. Int. Ed. 48, 321–324.
Singh, A., Gautam, P.K., Verma, A., Singh, V., Shivapriya, P.M., Shivalkar, S., Sahoo, A. K., Samanta, S.K., 2020. Green synthesis of metallic nanoparticles as effective alternatives to treat antibiotics resistant bacterial infections: A review. Biotechnol. Rep. 25, e00427.
Wang, P., Yang, J., Zhou, B., Hu, Y., Xing, L., Xu, F., Shen, M., Zhang, G., Shi, X., 2017. Antifouling manganese oxide nanoparticles: synthesis, characterization, and applications for enhanced MR imaging of tumors. ACS Appl. Mater. Interf. 9, 47–53.
Weiss, P.S., 2010. Nanoscience and nanotechnology: present and future. ACS Publications.
Yadav, V.K., Ali, D., Khan, S.H., Gnanamoorthy, G., Choudhary, N., Yadav, K.K., Thai, V. N., Hussain, S.A., Manhrdas, S., 2020. Synthesis and Characterization of Amorphous Iron Oxide Nanoparticles by the Sonochemical Method and Their Application for the Remediation of Heavy Metals from Wastewater. Nanomaterials 10, 1551.
Yang, H., Zhuang, Y., Hu, H., Du, X., Zhang, C., Shi, X., Wu, H., Yang, S., 2010. Silica-coated manganese oxide nanoparticles as a platform for targeted magnetic resonance and fluorescence imaging of cancer cells. Adv. Funct. Mater. 20, 1733–1741.